Phase transitions in flexible solution-processed ferroelectric P(VDF-TrFE) copolymer thin films

Simon Toinet, Mohammed Benwadih, Samuel Tardif, Joël Eymery, Christine Revenant

Phase Transitions in Flexible Solution-Processed Ferroelectric P(VDF-TrFE) Copolymer Thin Films

Simon Toinet[1], Mohammed Benwadih[1], Samuel Tardif[2], Joël Eymery[2], and Christine Revenant[2]*

[1]Univ. Grenoble Alpes, CEA, LITEN, 38000 Grenoble, France
[2]Univ. Grenoble Alpes, CEA, IRIG, MEM, NRS, 38000 Grenoble, France

Corresponding author: E-mail: christine.revenant@cea.fr

Abstract The polyvinylidene fluoride trifluoroethylene P(VDF-TrFE) copolymer is polymorphic with two main phases called α (paraelectric) and β (ferroelectric). Effects of annealing, cooling, and poling on the phase transitions are studied in thin films. More precisely, the α-β structural transition is investigated in copolymer capacitors with flexible electrodes and substrate using in situ synchrotron X-ray diffraction. After annealing above the Curie transition, another phase called δ is put in evidence during cooling as α transforms into β. With combined effect of annealing and poling, a sharp phase transition is put in evidence from β to δ at 96 °C after stopping poling (E = 70 MV m^{-1}) and a continuous phase transition occurs from δ to α in the range from 100 to 110 °C. The δ phase has high crystallinity with a domain size (normal to the film surface) of approximately 50 nm i.e. more than three times larger than for β. These phase transformations occur at relatively small electric field because of additional thermal effect and stress change for β and δ/α due to morphological changes. Permittivity and ferroelectric measurements performed on the copolymer capacitors allow confirming the phase transitions from β to δ and finally to α.

Keywords Annealing. Crystallinity. Ferroelectric properties. Phase transition. Poling. P(VDF-TrFE)

Introduction

Ferroelectric films are currently used in numerous applications like memories, microsystems, and high frequency electrical components [1]. Ferroelectric materials can be inorganic, like complex oxides [2-4] or organic like polyvinylidene fluoride (PVDF) polymer [5]. The PVDF-based polymers are easy to process, chemically stable, and highly biocompatible. Moreover,

PVDF-based flexible electronics have been demonstrated in non-volatile memories, energy-harvesting devices, and multifunctional sensors [6].

The PVDF and its copolymers like polyvinylidene fluoride trifluoroethylene P(VDF-TrFE) are semi-crystalline with different crystalline phases. In order to master the copolymer physical properties, it is essential to identify the thermal and electrical conditions for the stability of the phase transitions.

The PVDF crystallization from a solution or melt leads to the non-polar paraelectric α phase characterized by a trans-gauche-trans-gauche' (TGTG') conformation formed by ±60° dihedral angle between the neighboring monomer units. The electric dipoles cancelled out, as two polymer chains with alternating trans−gauche conformation TGTG' are packed antiparallel to each other in the unit cell. This stable thermodynamic phase at ambient temperature and pressure is favored by a slow cooling rate [7].

Another PVDF polymorph is the ferroelectric β phase with an orthorhombic crystal structure. For example, in case of 75 mol% VDF, the lattice parameters are a = 8.86 Å, b = 4.62 Å, and c = 2.55 Å [8]. This phase has an all-trans (all-T or TTTT) configuration formed by 180° dihedral angle between the neighboring monomer units i.e. planar zigzag. The dipoles are perpendicular to the carbon chain direction (c-axis) and crystalline fibrils parallel to the substrate surface are superimposed in the direction perpendicular to the surface [9]. Permanent dipoles with spontaneous polarization are along the b-axis [10]. Ferroelectric switching occurs by global rotation of the polymer chain axis (c-axis). The optimal annealing temperature is in the middle of Curie temperature T_c ranging from 95 °C to 115 °C and melting temperature T_m (~150 °C) [11]. At T_m, P(VDF-TrFE) becomes a viscous film. Short annealing time is enough to induce a high crystallinity degree and remnant polarization P_r. Indeed, longer annealing would not improve but rather deteriorate functionality [12]. Similarly, if the electric field is sufficiently strong, necessary poling is short [13]. When P(VDF-TrFE) is heated and then cooled to room temperature (RT), α phase is transformed into β phase, following a phase transition which is dependent on annealing and cooling rate [14]. Moreover, α phase is transformed into β phase by applying stress of 100-350 MPa [15].

For P(VDF-TrFE) (45-55) and at annealing up to 72 °C, the β-to-α phase transition proceeds through an intermediate γ phase [16].

There is also a polar version of α, called δ, which has been experimentally studied only in pure PVDF. Both phases have similar cell parameters and same chain conformation [7,17]. The δ-PVDF is orthorhombic with a = 4.96 Å, b = 9.64 Å, and c = 4.62 Å. So far, δ-PVDF has been elaborated by applying (i) high electric fields of 250 MV m^{-1} on as-deposited or annealed paraelectric films [18], (ii) high pressure on a PVDF powder at elevated temperatures [17] to get a coercive field E_c of 110 MV m^{-1} and a saturation polarization of 7 µC cm^{-2}, (iii) annealing

at 200 °C for 1 h followed by quenching [19] (the transition is only partial and P_r = 2.3 µC cm^{-2}), and (iv) high temperature annealing and short electrical pulses [18] to get P_r = 7 µC cm^{-2} and E_c = 115 MV m^{-1}. The dipole moment is along the *a*-axis and the polarization is stable at high temperatures [18]. Kim et al. have theoretically studied possible routes from α to β in bulk PVDF [20]. As the direct α-β transformation requires high energy, the transition proceeds through an intermediate phase. One prototypical route consists in transforming α to δ by intramolecular rotation of CH_2 upward and CF_2 downward about the G and G′ bonds, respectively and then in changing the TGTG′ conformation to an all-trans one [20]. This route starts with a low energy barrier at the α-δ transformation. The axial stress parallel to the chain direction becomes negative for the transformation from TGTG' to all-T and finally becomes positive for β. So far, δ phase has been put in evidence only starting from a paraelectric material.

Moreover, copolymers with a high ratio of VDF (70-80 mol%) exhibit improved ferroelectric behavior [8].

Although some studies have been done on phase transitions in PVDF-based polymers, no studies have been reported so far on δ phase in P(VDF-TrFE) copolymer. This paper brings insights in the α-β transition of P(VDF-TrFE) on a flexible substrate using in situ synchrotron X-ray diffraction (XRD) experiment first during annealing and cooling. Then, the ferroelectric-paraelectric phase transition from β to α through δ after short electrical pulses will be studied as a function of annealing. These structural behaviors will be correlated to the measured dielectric and ferroelectric properties of the materials.

Experimental

Film Preparation

We used the FC20P grade of P(VDF-TrFE) (80-20) synthesized by ARKEMA-Piezotech. The sample consists of a 50 µm thick layer of P(VDF-TrFE) deposited on a polyethylene naphthalate (PEN) substrate (125 µm).

Capacitor Fabrication

The bottom electrode was deposited by screen printing on a 125 µm thick PEN substrate and was annealed at 150 °C during 10 min. Then, the copolymer was printed and annealed at 60 °C. Finally, the upper electrode was deposited and annealed at 60 °C in order to start the in

situ XRD with the most amorphous device as possible. The P(VDF-TrFE) layer is 3.5 µm thick and the PEDOT:PSS electrodes are 1 µm thick.

X-Ray Diffraction

The XRD measurements were performed on the BM32 beamline at the European Synchrotron Radiation Facility (ESRF, Grenoble, France) in the $\theta/2\theta$ geometry. The incident energy was set to 27 keV (λ = 0.4592 Å) to minimize absorption by the sample and hence degradation by X-rays. The diffraction pattern was collected on a 2D detector with a high-resolution $\Delta q = 2.36.10^{-3}$ Å^{-1}. For in situ annealing, samples were placed on a Si wafer on a hot plate (Anton Paar DHS 900) used in the ambient air. The temperature of the hot plate is called furnace temperature T_f. and the sample temperature T_s was measured by a thermocouple fixed on the sample surface with a copper tape. The sample was either the P(VDF-TrFE) film or the P(VDF-TrFE) based capacitor. The correspondence between both temperatures is given in Fig. S1 and Table S1 (Supporting Information). In case of no specific indication in the article, temperature corresponds to T_s. Additionally, poling was performed by applying sinusoidal voltage. During the capacitor study as a function of annealing, a succession of 150 V (42.9 MV m^{-1}), 200 V (57.1 MV m^{-1}), and 250 V (71.4 MV m^{-1}) poling at 10 Hz was applied during 10 cycles for each voltage at a given temperature. The capacitor was heated up to T_f = 155 °C and poling was applied up to T_f = 129 °C. The XRD measurements were performed in situ.

Permittivity and ferroelectric measurements

Capacitance and resistance were measured with a E4980A capacitor meter (Agilent). The capacitors were heated on a MK 1000 hot plate (Instec), temperature was measured by a 23XT multimeter (WavetekMeterman) and a K type thermocouple (TC Direct). The polarization-electric field (*P*-*E*) hysteresis loops were measured by a Precision Multiferroic II Ferroelectric Test System (Radiant technologies). The capacitors were heated on a PZ28-2 hot plate (Präzitherm), temperature was measured by a 23XT multimeter (WavetekMeterman) and a K type thermocouple (TC Direct). The correspondence between both temperatures T_f and T_s is given in Table S2 (Supporting Information). As a first step, samples were put on the PZ28-2 hot plate. Second, they were polarized by a 250 V_{peak} sinusoidal signal during 1 min, then (*P*-*E*) hysteresis loops were measured by using a 250 V_{peak} sinusoidal signal. The polarization and (*P*-*E*) measurements were performed at low frequency (0.1 Hz). All the measurements could not be performed on the same test bench. To prevent from cooling, samples were transported on the MK 1000 hot plate for the capacitance and resistance measurements. Capacitance and resistance were measured at 20 Hz. The procedure was repeated for each

temperature between 59 °C and 94 °C. After 94 °C, there was no polarization before the measurements.

Results and discussion

Phase evolution of P(VDF-TrFE) film as a function of temperature

In situ XRD data are shown in Fig. 1a during annealing and cooling.

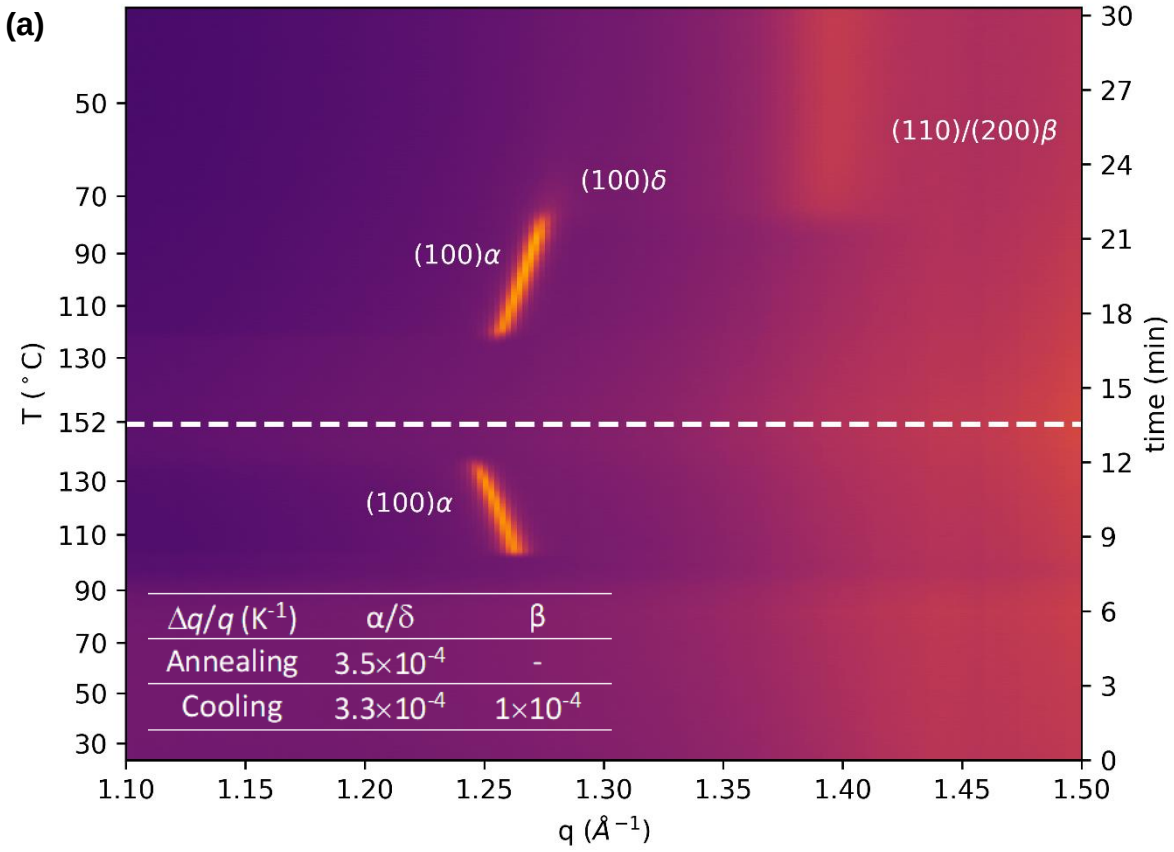

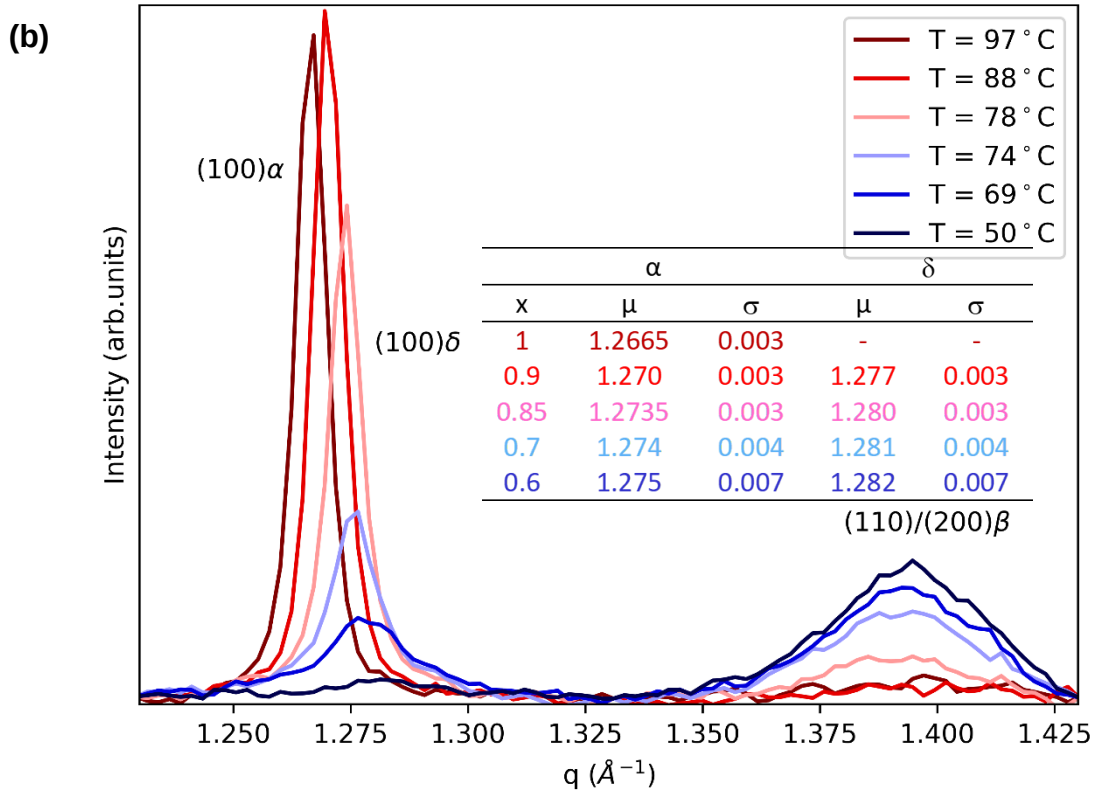

	α		δ	
x	μ	σ	μ	σ
1	1.2665	0.003	-	-
0.9	1.270	0.003	1.277	0.003
0.85	1.2735	0.003	1.280	0.003
0.7	1.274	0.004	1.281	0.004
0.6	1.275	0.007	1.282	0.007

Fig. 1 In situ XRD as a function of temperature **a** during annealing from T_f = 25 °C to 152 °C and during cooling from T_f = 152 °C to 40 °C and **b** horizontal cuts of the image **a** at several T_s from 97 °C to 50 °C. Inset of **a**: $\Delta q/q$ of the α/δ and β peaks during annealing and cooling. Inset of **b**: fit parameters of the α/δ peak with x the α fraction, μ the mean value, and σ the standard deviation of the Gaussian function for α and δ

As T_f reaches approximately 110 °C, an XRD peak appears at q smaller than 1.3 Å^{-1} and corresponds to (100)α. As T still increases, the peak slightly moves towards smaller q, corresponding to a larger interplanar distance in direct space. This peak vanishes at T_f = 140 °C close to T_m, where P(VDF-TrFE) becomes disordered. It is checked that upon cooling (see the upper part of the Fig. 1a) the (100)α peak reappears at T_f = 125 °C. Horizontal cuts of this figure show the detailed peak profile evolution as a function of T (Fig. 1b). As T still decreases, the (100)α peak slightly moves towards higher q. In direct space, this corresponds to a smaller interplanar distance due to thermal contraction. Then, at T_s = 78 °C, the peak at q = 1.275 Å^{-1} decreases and is asymmetric. This asymmetry comes from the α phase contribution at small q and the δ phase one at high q. The peak is fitted with two Gaussian functions for α and δ (fit parameters in the inset of Fig. 1b). As T decreases, the δ fraction increases, both mean values μ slightly increase, and both standard deviations σ increase. Moreover, another peak at q = 1.4 Å^{-1} appears at 78 °C and corresponds to the (110)/(200) β phase. This phase appears as δ exists. At 69 °C, both contributions of α and δ are clearly visible at 1.275 and 1.282 Å^{-1} respectively. Finally, at 74-50 °C, the δ peak vanishes and the β peak increases. The phase transition occurs progressively with the decrease/disappearance of δ and the apparition/growth of β. Globally, the α/δ peak is narrow indicating large domains, whereas the β peak is wide indicating small domains. The thermal evolution of the peak allows determining the $\Delta q/q$ parameter, i.e. the $\Delta d/d$ parameter (d: interplanar spacing) which is different for α/δ and β (inset of Fig. 1a).

As the phase evolution may be different during first/second annealing [14], in situ XRD measurements were performed during a second heat treatment on the same sample (Fig. 2a).

(a)

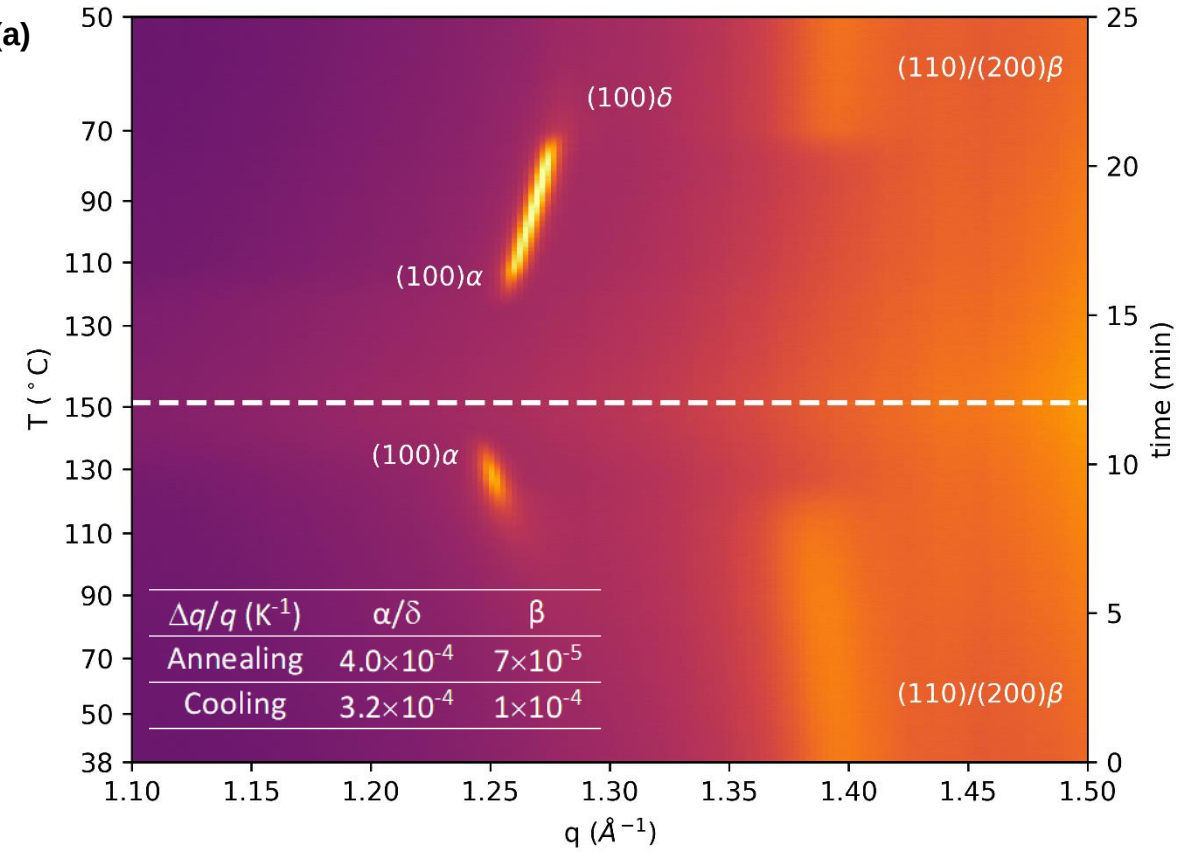

(b)

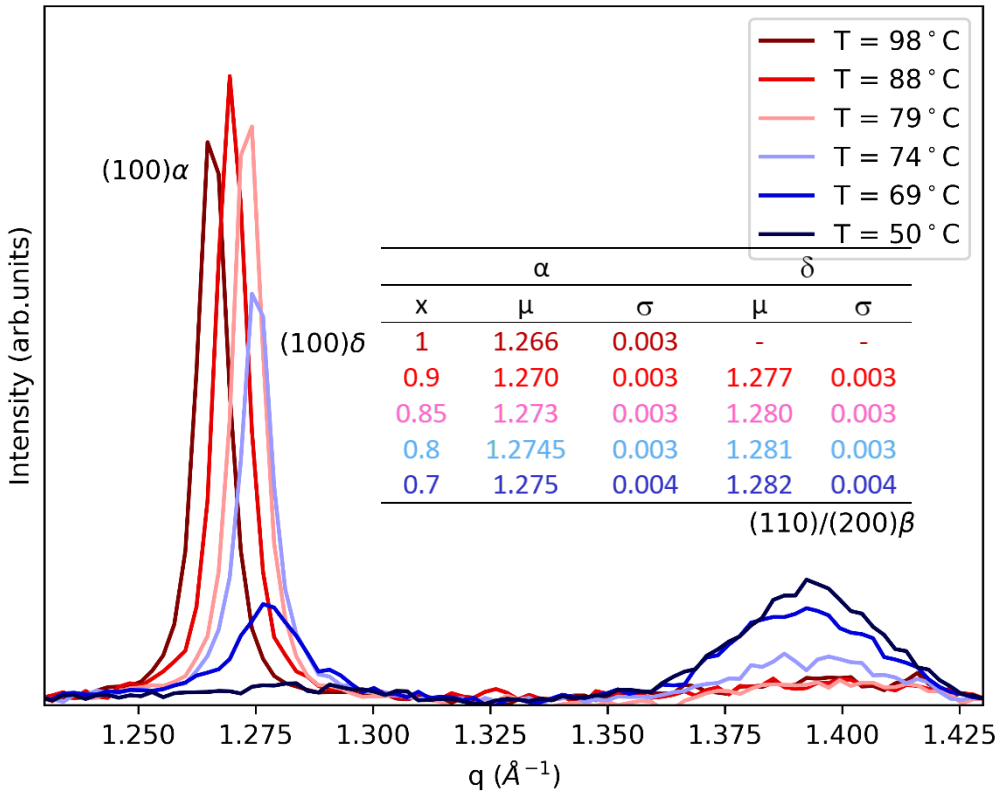

	α		δ	
x	μ	σ	μ	σ
1	1.266	0.003	-	-
0.9	1.270	0.003	1.277	0.003
0.85	1.273	0.003	1.280	0.003
0.8	1.2745	0.003	1.281	0.003
0.7	1.275	0.004	1.282	0.004

(110)/(200)β

Fig. 2 In situ XRD as a function of temperature **a** during the second heat treatment from T_f = 38 °C to 150 °C and during cooling from T_f = 150 °C to 50 °C, **b** horizontal cuts of the image **b** at several T_s from 98 °C to 50 °C. Inset of **a**: $\Delta q/q$ of the α/δ and β peaks during annealing and cooling. Inset of **b**: fit parameters of the α/δ peak

At low temperature, we measured only the β peak (Fig. 2a). This peak remains approximately at the same q position as T increases. The thermal stress between the layer and the substrate is:

$$\sigma = \frac{E(\alpha_s - \alpha_l)\Delta T}{1-\nu} \quad (1)$$

where E is the Young's modulus, ν is Poisson's ratio, α_l and α_s are the CTE of the layer and substrate respectively. In this definition, a positive (negative) value of stress means the layer is under tensile (compressive) stress. As the crystalline domains are densely packed at low temperature, the macroscopic strain behaviour of the material is identical to that of the crystalline domains [21]. The $\Delta d/d$ parameter of β (inset of Fig. 2a) is smaller than the CTE of the PEN substrate estimated to 1.7×10^{-4} K^{-1} by using the XRD curves from 25 °C to 145 °C (Fig. S2, Supplementary Information), in good agreement with that mentioned in literature (~10^{-4} K^{-1}) [22]. During annealing, the PEN substrate tries to impose an expansion of the P(VDF-TrFE) film parallel to the surface, β is under in-plane tension (positive stress) that is compensated by shrinking in the out-of-plane direction. This contraction is of the same order of magnitude than the out-of-plane intrinsic dilatation due to annealing, explaining why the β peak remains approximately at the same q position. Upon further annealing, the β peak decreases and a peak at q = 1.26 $Å^{-1}$ (α) appears at 117 °C. At 126 °C, the β peak disappears and finally, the α peak disappears at T_f = 145 °C. Then, the sample is cooled from T_f = 150 °C to 50 °C. The α peak appears at T_f = 125 °C and the peak shifts towards high q. Fig. 2b shows that the high-q limit of this peak remains at q = 1.28 $Å^{-1}$, as the low-q limit shifts towards high q. This peak is fitted with two Gaussian functions for α and δ (fit parameters in the inset of Fig. 2b). As T decreases, the δ fraction increases, both mean values μ slightly increase, and both standard deviations σ slightly increase at low T. Regarding the β peak, it appears at 74 °C. The CTE of the PEN substrate is estimated to 1.5×10^{-4} K^{-1} during cooling by using the XRD curves from 145 °C to 25 °C (Fig. S2, Supplementary Information).

P(VDF-TrFE) behaves differently during the first or second experiment, indicating that the present phases depend on thermal history. The main difference is the β phase existence at beginning of annealing during the second experiment. Indeed, β phase is generated at the end

of the first experiment during cooling. The $\Delta d/d$ parameter of β (resp. α/δ) is smaller (resp. larger) than the CTE of the PEN substrate. Moreover, the main result is the apparition of δ in P(VDF-TrFE) during cooling in the first and second experiments without any applied electric field during the transition from α to β.

Capacitor as a function of poling voltage and frequency

In situ XRD data of the P(VDF-TrFE) capacitor are shown in Fig. 3 as a function of poling voltage at T_s = 71 °C and at 1 Hz.

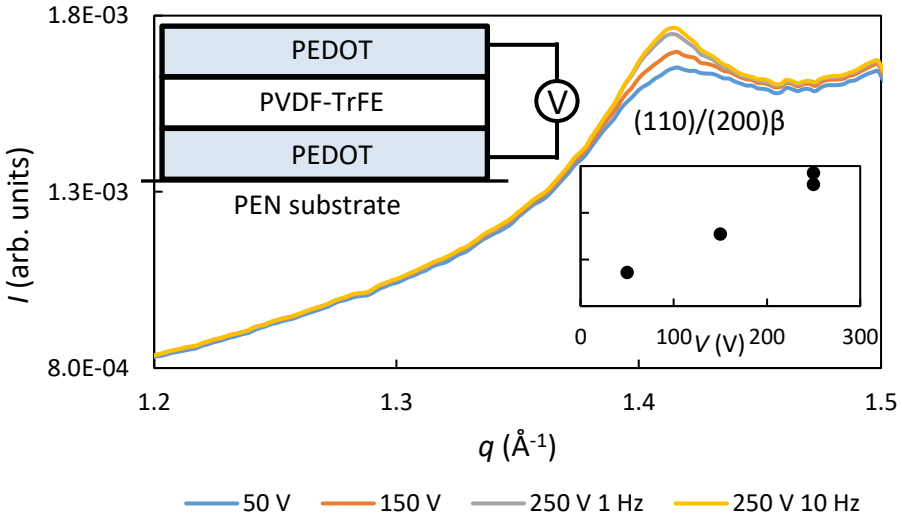

Fig. 3 In situ XRD of the P(VDF-TrFE) capacitor at 71 °C as a function of poling voltage (50, 150, and 250 V) at 1 Hz and as a function of poling frequency (1 and 10 Hz) at 250 V. Insets: Schematics of the P(VDF-TrFE) capacitor sandwiched between two PEDOT:PSS electrodes on the PEN substrate and intensity of the β peak as a function of the poling voltage.

There is only one peak at q = 1.41 Å^{-1} corresponding to (110)/(200)β phase. The inset of Fig. 3 shows that the peak intensity increases linearly in the range 50-250 V at 1 Hz. Additional poling at 250 V and 10 Hz slightly increases the β phase contribution.

Capacitor during annealing and poling

In situ XRD data during annealing up to T_s = 100 °C are shown in Fig. 4a.

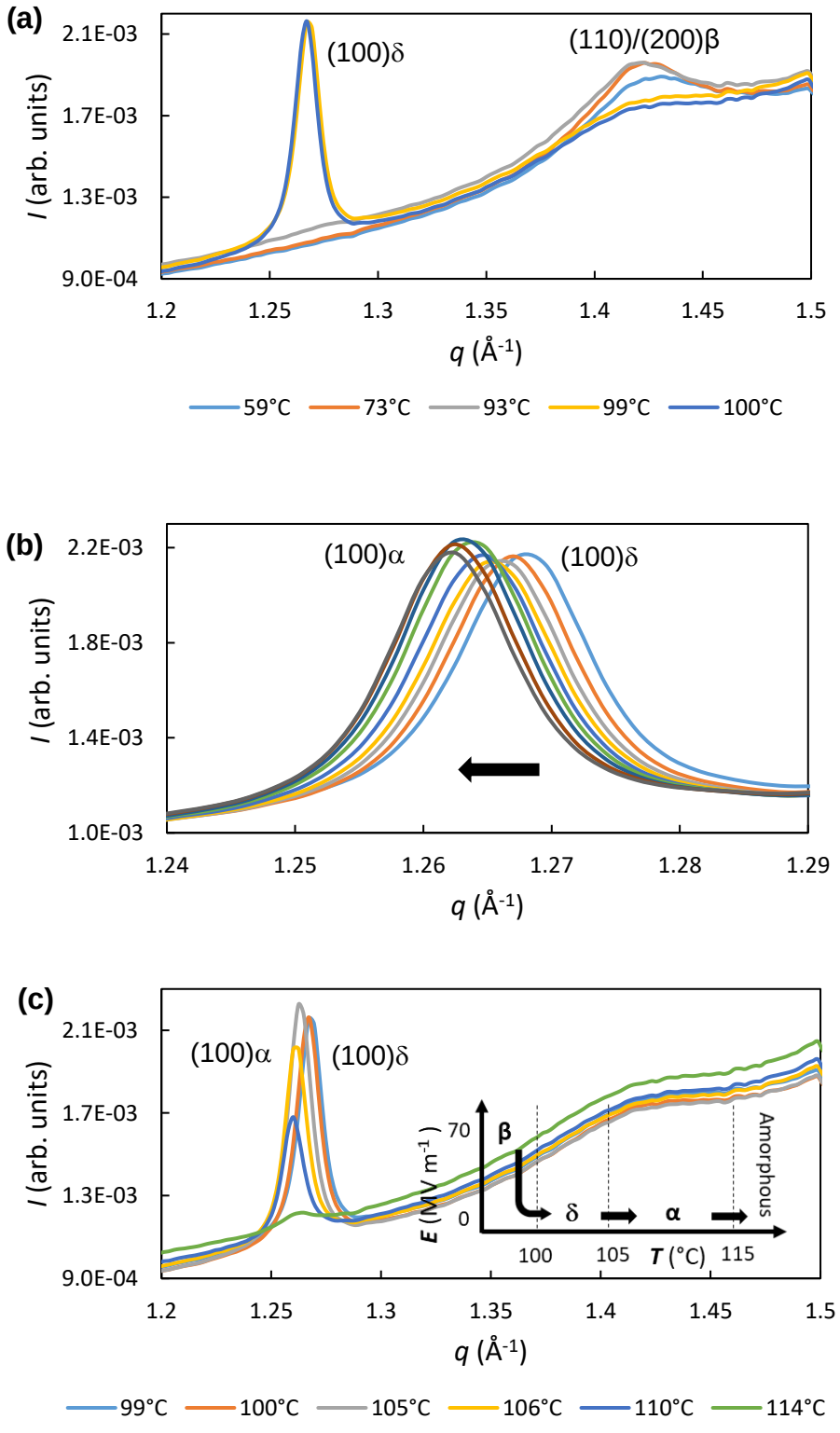

Fig. 4 In situ XRD of the P(VDF-TrFE) capacitor during annealing **a** up to T_s = 100 °C (poling is applied up to 94 °C), **b** from 99 °C to 107 °C (ΔT = 1 °C), detailed view of the low-q peak, and **c** from 99 °C to 114 °C. Inset: Electric field-temperature (E-T) phase diagram of P(VDF-TrFE)

At 59 °C, there is only a wide (110)/(200)β peak indicating small β crystalline domains. The domain size (normal to the film surface), calculated from the full width at half maximum (FWHM) using the Scherrer formula, is approximately 12 nm (resp. 16 nm) at 59 °C (resp. 73 °C) (Table S3, Supporting Information). In this temperature range, the lattice parameter *a* is 8.80-8.83 Å, similar to *a* = 8.86 Å found for a similar composition (75 mol% VDF) [8]. The β peak intensity increases up to 93 °C when electric field is still present. Once poling stops, the β peak disappears at 99 °C and a peak at q = 1.27 $Å^{-1}$ corresponding to (100)δ appears in an abrupt way. The δ peak is quite intense and narrow, indicating quite large domain size, i.e. 46 nm at 101 °C (see Table S3, Supporting Information). Therefore**,** the δ crystalline domains are larger by a factor 3-4 than the previous β ones. In this study, δ is obtained with a maximum electric field of 70 $MV.m^{-1}$, more than three times less than what was used by Li et al starting from α phase [18]. According to Kim et al., the energy barrier from α to δ is 21 meV/CH_2CF_2 unit, similar to that from β to δ (20 meV/CH_2CF_2 unit at 70-100 MV m^{-1}) [20]. Consequently, the much lower electric field necessary in our case is attributed to the additional thermal effect. The δ peak maximum slightly shifts towards smaller *q*, corresponding to a larger distance. Near T_c, crystalline domains are embedded in a quite large amount of amorphous phase with a Young's modulus much lower than that of the crystalline domains [21]. We show that the thermal behavior at the crystalline domain nanoscale depends on the phase and may be different from the macroscopic thermal behavior of the P(VDF-TrFE) film. During annealing, the PEN substrate tries to impose an expansion on the P(VDF-TrFE) film parallel to the surface. As the amorphous phase should follow this expansion, we propose that the δ crystalline domain evolution is quite uncorrelated from the substrate expansion, explaining the $\Delta d/d$ difference between β and δ. As the δ crystalline domains are quite free to expand, $\Delta d/d$ corresponds to the CTE of δ. The decrease of in-plane expansion of the crystalline domains helps modifying the P(VDF-TrFE) backbone i.e. changing the all-T conformation (β) to the TGTG' one (δ). In bulk PVDF, the axial stress parallel to the chain direction is first positive and then decreases during the route from β to δ [20]. Figure 4b shows a detailed view of the low-*q* peak from T_s = 99 °C to 107 °C. The peak moves towards smaller *q*, first decreases slightly from 100 °C to 102 °C before increasing from 103 °C to 105 °C. This continuous peak evolution corresponds to a phase transition from δ to α. Hence, δ makes the transition from β to α (cf. inset of Fig. 4c). Then, the δ peak decreases above 106 °C. As temperature still increases, the peak goes on shifting towards smaller *q* (Fig. 4c). More precisely, the low-*q* limit of the peak remains at q = 1.26 $Å^{-1}$, as the high-*q* limit shifts towards low *q*. This indicates that, at this stage, the predominant peak contribution is α. With correction of the PEN thermal dilatation, the maximum of the δ/α peak slightly shifts towards smaller *q*, corresponding to larger distances (Fig. S4, Supporting Information). Furthermore, α peak is narrow, indicating large α

domain size (49 nm at 110 °C) (Table S3, Supporting Information). Ultimately, the α peak nearly disappears at 114 °C.

Let us estimate the thermal stress at the β-δ transition. Using a Poisson's ratio ν of 0.34, a macroscopic Young's modulus E of 0.4 GPa [21] at 96°C, the CTE of the PEN substrate determined by XRD and the macroscopic CTE of P(VDF-TrFE) = 1.22×10^{-4} K^{-1} [23], Equation (1) yields a thermal stress of 2.2 MPa.

In P(VDF-TrFE) capacitor, a well-crystallized δ phase has been obtained at approximately 99-103 °C with an electric field of 70 MV m^{-1} up to 94 °C. The temperature used is much lower than that used by Garcia-Zaldivar et al. [19] and the electric field used is much lower than that used by Li et al. [18]. The main reason is the interplay between temperature and electric field in our case. During annealing only, the β-α transition occurs progressively at 117 °C. On the contrary, with combined thermal and electric effect, the β-δ-α transition occurs suddenly as soon as the electric field is stopped at 94 °C. Hence, applying or not electric field has an important effect on the phase transition during annealing.

In order to show that δ can have an impact on the properties, permittivity and ferroelectric measurements were performed with/without E as a function of T.

Permittivity measurements

The thermal evolution of the permittivity is displayed in Fig. 5 at different frequencies without polarization and with a 250 V polarization. In both cases, permittivity decreases as frequency increases. The permittivity has a broad maximum corresponding to T_{c1} = 93 °C. The maximum permittivity value depends on the probing frequencies but the temperature at which the maximum takes place (T_{c1}) is frequency independent. In contrast, the dielectric spectra obtained for P(VDF-TrFE) with a larger TrFE percentage such as 55 mol% are frequency-dependent because of the relaxor ferroelectric behavior which stems from the TrFE units [24].

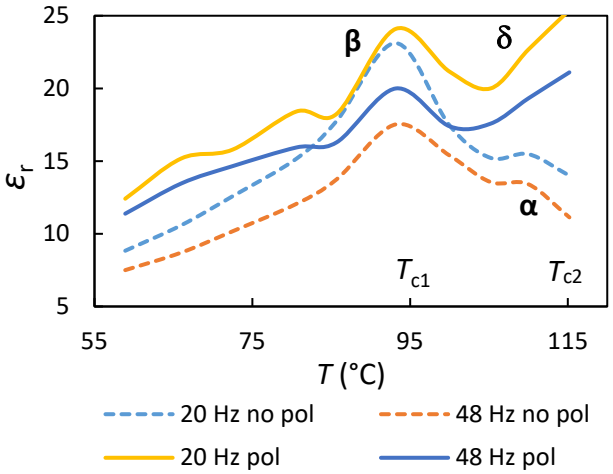

Fig. 5 Permittivity properties of P(VDF-TrFE). Permittivity as a function of T_s during annealing at different frequencies without any polarization and with a 250 V polarization

With a 250 V polarization, the permittivity maximum is 24 at 20 Hz. At T_{c1}, β phase is present (Fig. 4a). Above this temperature, permittivity first decreases and then increases whatever the frequency. This may correspond to a second phase transition (T_{c2} = T_{c1}+20) in link with δ. Without polarization, the permittivity maximum corresponding to β is still present, then at high temperature, permittivity decreases and there is a slight bump at 110 °C. At this temperature, the permittivity is equal to 15, in agreement with the value of 15 found in similar conditions for P(VDF-TrFE) [25]. In this thermal range, α phase succeeds to β phase.

Ferroelectric property measurements

Figure 6 shows the *P-E* loops for P(VDF-TrFE) at 0.1 Hz at several T_s.

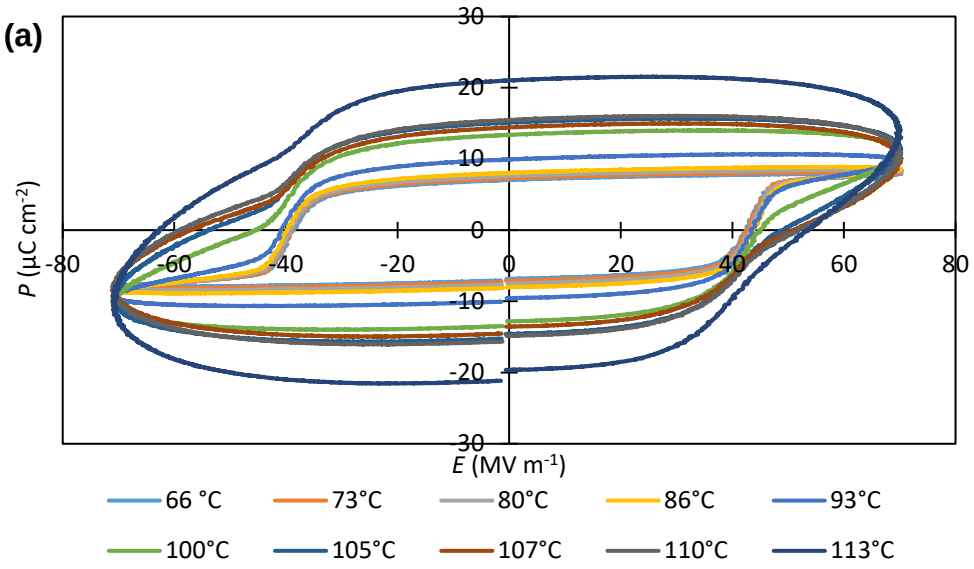

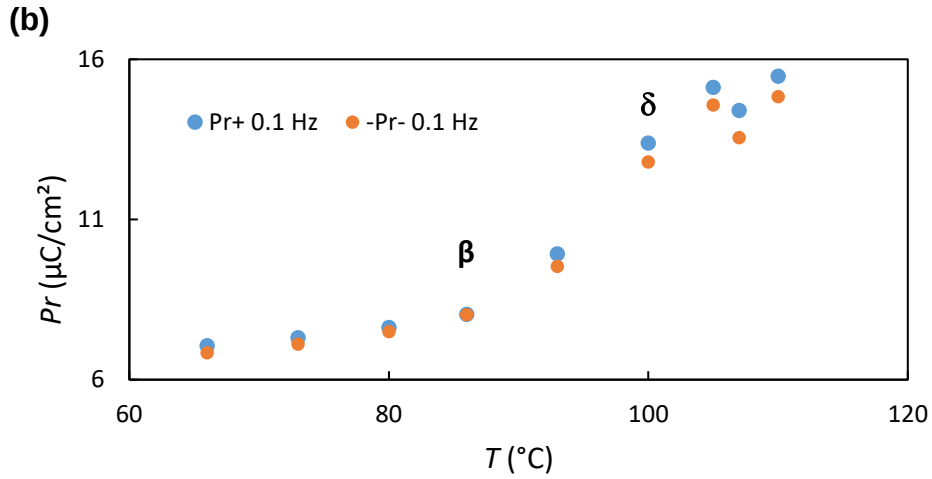

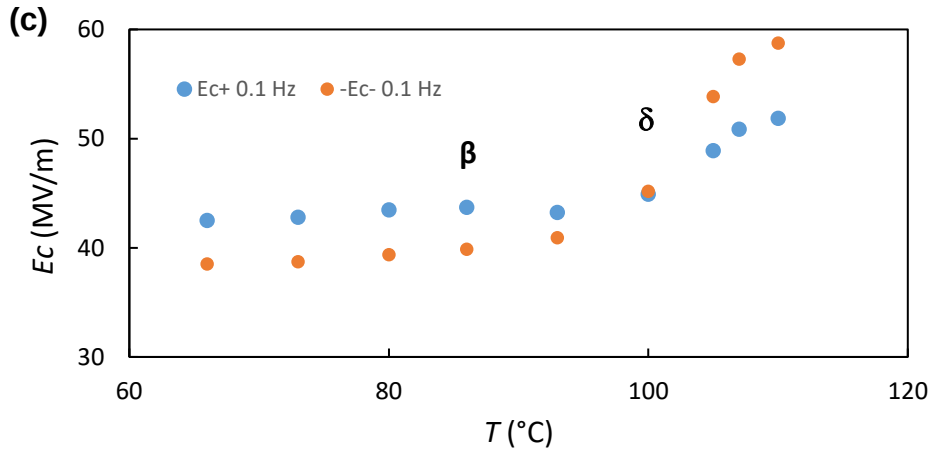

Fig. 6 Ferroelectric properties of P(VDF-TrFE) at 0.1 Hz. **a** Hysteresis *P-E* loop at several T_s, **b** remnant polarization P_r, and **c** coercive field E_c as a function of T_s

The *P-E* loops display non-linear ferroelectric behavior with saturation up to 100 °C (Fig. 6 a). Above, the hysteresis loops become gradually more rounded and at 113 °C, the *P-E* loop corresponds to a lossy capacitor (α phase). The parameters P_r and E_c plotted in Fig. 6b and c for non-linear ferroelectric *P-E* loops (up to 110 °C) increase with *T*. As the [110] and/or [200] directions of β are mostly perpendicular to the surface (Fig. 4a), only the projection of the dipole moment (*b*-axis oriented) on the [110] direction yields P_r. At the β-δ transition, P_r jumps from 9-10 μC cm^{-2} to 13 μC cm^{-2}, confirming the sharp phase transition. As the [100] direction of δ is perpendicular to the surface (Fig. 4b), the dipole moment (*a*-axis oriented) yields P_r. Hence, the difference of dipole orientation between β and δ explains the P_r increase at the transition. This last P_r value for δ is larger than those of 7 μC cm^{-2} and 2.3 μC cm^{-2} reported for PVDF [18,19] and that of 4.5 μC cm^{-2} for 30 μm thick P(VDF-TrFE) 65/35 mol% films [26]. These films show similar P_r increase as a function of *T* [26]. Note that E_c increases above 100 °C for δ. Indeed, a higher electric field is necessary to switch the δ dipoles perpendicular to the surface compared to the β ones. In our case, E_c is equal to 50 MV m^{-1}, approximately half of that reported for δ in PVDF [17,18]. A different thermal evolution of P_r and E_c is observed for PVDF comprising β crystals, isotropic amorphous phase, and oriented amorphous phase stemming from the large-scale plastic deformation of the biaxially oriented PVDF [27]. For such PVDF films, P_r (resp. E_c) decreases above 100 °C (resp. 75 °C). The P_r evolution is attributed to a decrease of the ferroelectric domain size with increasing temperature. Note that P(VDF-TrFE) has been primarily introduced mainly to ease the β crystal formation without plastic deformation. The elaboration difference between PVDF and P(VDF-TrFE) explains the difference in structure and property evolution with increasing temperature. In our case, the ferroelectric properties of δ P(VDF-TrFE) are attributed to the large domain size and to the dipole moment orientation perpendicular to the surface. In short, the dielectric and ferroelectric measurements confirm that δ phase in P(VDF-TrFE) occurs at 100-105 °C after having applied an electric field of 250 V.

Conclusions

This study puts in evidence the thermal and poling conditions for the stability/transitions of the different copolymer phases. During cooling after annealing above T_c, δ phase appears in P(VDF-TrFE) films at the transition from α to β. After short electrical pulses of relatively low electric field (70 MV m^{-1}), a sharp phase transition occurs from β to δ during annealing at 96 °C. The dielectric and ferroelectric measurements confirm that δ occurs in the range 100-105 °C after having applied a 70 MV m^{-1} AC electric field. The thermal stress at the crystalline domain nanoscale depends on the phase and may be different from the macroscopic thermal

one. The low electric field necessary for the β-δ phase transformation is due to the additional thermal effect and stress change in the copolymer film during annealing. In addition, Fourier Transform InfraRed (FTIR) experiments are planned in order to get complementary information about the different phases of PVDF-based polymers. Applying or not electric field has an important effect on the phase transition during annealing. The described structural and electrical study is important in order to master the stability/transitions of the different crystalline phases as a function of annealing, cooling, and poling for technological applications.

Acknowledgments We would like to thank Christophe Serbutoviez and Audrey Martinent for their support, David Alincant for process and Fabrice Domingues Dos Santos for supplying P(VDF-TrFE) polymer. We acknowledge the French CRG committee for provision of synchrotron radiation beamtime and we would like to thank the staff of BM32.

Declarations

Conflict of Interests The authors declare that they have no competing interests.

References

1. Setter N, Damjanovic D (2006) J Appl Phys 100:051606
2. Gao W, Zhu Y, Wang Y, Yuan G, Liu J-M (2020) Journal of Materiomics 6:1
3. Mansour C, Benwadih M, Chahine GA, Revenant C (2020) AIP Adv 10:065204
4. Mansour C, Benwadih M, Revenant C (2021) AIP Adv 11:085302
5. Asadi K (2022) Organic Ferroelectric Materials and Applications, Ed. Asadi K, Elsevier
6. Chen X, Han X, Shen Q-D (2017) Adv Electron Mater 3:1600460
7. Su H, Strachan A, Goddard WA (2004) Phys Rev B 70:064101
8. Ohigashi H, Koga K (1982) Jpn J Appl Phys 21:L455-L457
9. Aliane A, Benwadih M, Bouthinon B, Coppard R, Domingues-Dos Santos F, Daami A (2015) Org Electron 25:92–98
10. Kepler RG, Anderson RA (1992) Adv Phys, 41:1-57
11. Li Y, Feng W, Meng L, Tse KM, Li Z, Huang L, Su Z, Guo S (2021) Materials and Design 199:109415
12. Spampinato N, Maiz J, Portale G, Maglione M, Hadziioannou G, Pavlopoulou E (2018) Polymer 149:66–72
13. Ducrot P-H, Dufour I, Ayela C (2016) Sci Rep 6:19426
14. Oliveira F, Leterrier Y, Manson J-A, Sereda O, Neels A, Dommann A, Damjanovic D (2014) J Polym Sci, Part B: Polym Phys 52:496-506

15. Bassett DC (1982) Developments in Crystalline Polymers-I, Ed. Bassett DC, Applied Science, London
16. Pramanick A, Misture S, Osti NC, Jalarvo N, Diallo SO, Mamontov E (2017) Phys Rev B, 96:174103
17. Martin J, Zhao D, Lenz T, Katsouras I, de Leeuw DM, Stingelin N (2017) Mater Horiz 4:408
18. Li M, Wondergem HJ, Spijkman M-J, Asadi K, Katsouras I, Blom PWM, de Leeuw DM (2013) Nat Mater 12:433
19. Garcia-Zaldivar O, Escamilla-Diaz T, Ramirez-Cardona M, Hernandez-Landaverde MA, Ramirez-Bon R, Yanez-Limon JM, Calderon-Pinar F (2017) Sci Rep 7:5566
20. Kim WJ, Han MH, Shin Y-H, Kim H, Lee EK (2016) J Phys Chem B 120:3240
21. Hafner J, Benaglia S, Richheimer F, Teuschel M, Maier FJ, Werner A, Wood S, Platz D, Schneider M, Hradil K, Castro FA, Garcia R, Schmid U (2021) Nat Commun 12:152
22. Zoo Y, Adams D, Mayer JW, Alford TL (2006) Thin Solid Films 513:170
23. Jeung W-K, Choi S-M, Kim Y-J (2006) Journal of Electrical Engineering and Technology 1:263
24. Liu Y, Zhang B, Xu W, Haibibu A, Han Z, Lu W, Bernholc J, Wang Q (2020) Nat Mater 19:1169
25. Meng N, Zhu X, Mao R, Reece MJ, Bilotti E (2017) J Mater Chem C 5:3296
26. Katsouras I, Asadi K, Li M, van Driel TB, Kjaer KS, Zhao D, Lenz T, Gu Y, Blom PWM, Damjanovic D, Nielsen MM, de Leeuw DM (2016) Nat Mater 15:78
27. Huang Y, Rui G, Li Q, Allahyarov E, Li R, Fukuto M, Zhong G-J, Xu J-Z, Li Z-M, Taylor PL, Zhu L (2021) Nat Commun 12:675